Effect of Lattice Mismatch on the Magnetic Properties of Nanometer-Thick $La_{0.9}Ba_{0.1}MnO_3$ (LBM) Films and LBM/$BaTiO_3$/LBM Heterostructures

P. Mirzadeh Vaghefi[a,*], A. Baghizadeh[b], M. Willinger[c], A.A.C.S. Lourenço[a], V.S. Amaral[a]

[a]Department of Physics and CICECO, University of Aveiro, 3810-193 Aveiro, Portugal

[b]Department of Materials and Ceramics Engineering and CICECO, University of Aveiro, 3810-193 Aveiro, Portugal

[c]Fritz Haber Institute, Max Planck Society, Department of Inorganic Chemistry, Berlin, Germany.

Email address: pegah.mirzadeh@ua.pt (P. Mirzadeh Vaghefi)

Preprint submitted to Journal of Applied Surface Science July 28, 2017

Abstract

Oxide multiferroic thin films and heterostructures offer a wide range of properties originated from intrinsic coupling between lattice strain and nanoscale magnetic/electronic ordering. $La_{0.9}Ba_{0.1}MnO_3$ (LBM) thin-films and LBM/$BaTiO_3$/LBM (LBMBT) heterostructures were grown on single crystalline [100] silicon and [0001] Al_2O_3 using RF magnetron sputtering to study the effect of crystallinity and induced lattice mismatch in the film on magnetic properties of deposited films and heterostructures. The thicknesses of the films on Al_2O_3 and Si are 70 and 145 nm, respectively, and for heterostructures are 40/30/40 nm on both substrates. The microstructure of the films, state of strain and growth orientations was studied by XRD and microscopy techniques. Interplay of microstructure, strain and magnetic properties is further investigated. It is known that the crystal structure of substrates and imposed tensile strain affect the physical properties; i.e. magnetic behavior of the film. The thin layer grown on Al_2O_3 substrate shows out-of-plane compressive strain, while Si substrate induces tensile strain on the deposited film. The magnetic transition temperatures (Tc) of the LBM film on the Si and Al_2O_3 substrates are found to be 195 K and 203 K, respectively, slightly higher than the bulk form, 185 K. The LBMBT heterostructure on Si substrate shows drastic decrease in magnetization due to produced defects created by diffusion of Ti ions into magnetic layer. Meanwhile, the T_c in $LBMBT_s$ increases in respect to other studied single layers and heterostructure, because of higher tensile strain induced at the interfaces.

1. Introduction

The field of multiferroics has seen a revival of scientific and technological interest. Multiferroic materials are known to possess more than one ferroic order parameter, where

most of early works on this class of materials were done on structural magnetic ferroelectrics [1,2]. Research on multiferroics has involved efforts in artificial magnetoelectrics that consists of nano scale films compromising ferromagnetic and ferroelectric materials wherein magnetoelectric phenomena is stablished through interfaces strain [3]. In heterostructures the substrate/film interfaces or ferro-magnetic/ferroelectric interfaces become critically important for technological applications. Previous studies have showed the effect of misfit strain caused by lattice mismatch on magnetic and electric properties of films and heterostructures [4].

Since the observation of colossal magnetoresistance (CMR) effect in La-doped manganese oxides, they have been extensively investigated [5–7]. $La_{1-x}AE_xMnO_3$ (AE = alkaline earth) present a wide range of crystal structure and functionalities [2,8–10,4]. The overlap between Mn d orbitals and oxygen p orbitals produces an electronically active band, which can be influenced by the internal stress caused by AE-site substitution [11]. Particularly they are of current interest because in the regime of $x < 0.5$ they show fully spin polarized ferromagnetic metallic behavior at low temperature and paramagnetic insulator at high temperature [12]. Furthermore, biaxial strain due to the lattice mismatch between thin film and substrate plays a crucial role in controlling the physical proper-ties of thin films, such as Curie temperature (T_c) and magnetic anisotropy [13,14].

As a potential candidate for application among these groups of materials, Ba substitution of $LaMnO_3$($La_{1-x}Ba_xMnO_3$, referred as LBM hereafter) reveal room-temperature CMR effect [6,5] and higher T_c in low doping level than other CMR systems [7,15,16]. It was shown that $La_{0.7}Ba_{0.3}MnO_3/SrTiO_3$superlattice reduces T_c due to compressive strain [17], while $La_{0.8}Ba_{0.2}MnO_3/SrTiO_3$ enhances T_c due to the tensile strain in the film [18].

$BaTiO_3$ as a traditional ferroelectric is known for its unique piezoelectric behavior, which its diversity of phase transition makes it ideal for scientific research on mechanisms of wide range of structural transition phenomena [4,19,20].

In this paper, we studied the structural and magnetic proper-ties of strained LBM thin films with doping level of $x = 0.1$, grown on [0001]- Al_2O_3 and [100]-Si substrates and LBM/$BaTiO_3$/LBM (LBMBT) heterostructures on the same substrates. By comparing the lattice parameters of LBM target and used substrates ($a = 4.757$Å for Al_2O_3 and $a = 5.431$˚A for Si) the lattice mismatch in LBM/Al_2O_3 (LBM_a) and LBM/Si (LBM_s) can be derived as $\delta_{LBMa}=-0.18\%$ and $\delta_{LBMs}=-0.03\%$. The effect of microstructure of strained film on magnetic properties of the films well be accordingly discussed.

2. Experimental details

$La_{0.9}Ba_{0.1}MnO_3$(LBM) thin films were deposited on [0001]- Al_2O_3 and [100]-Si substrates by RF magnetron sputtering technique. The substrates were cleaned by acetone and ethanol to remove any kind of impurities on the surface. The deposition process was carried out in a gas mixture of 90% argon and 10% oxygen and a total pressure of 5.5 mTorr, in substrate temperature range of 700–750˚C.

To prove the presence of all elements in the films we have used Rutherford Backscattering Spectroscopy (RBS), where He^+ ions with incident energy of 2000 keV normal to the

sample surface and scattering angle of 140° were used to acquire the data. SIMNRA 6.06 software [21] was used to evaluate the spectra. According to the Kinematic theory of RBS, the energy of backscattered He^+ ions from the sample can be used to identify elements in the films [22]. According to RBS results, all analyzed films show corresponding peaks of La, Ba, Mn and oxygen in the deposited samples. The crystallinity of the films and heterostructures were studied with X-ray diffraction technique by a Philips X-Pert MRD® diffractometer in θ-2θ Bragg–Bentano geometry using $Cu_{k\alpha}$ radiation (λ_α= 1.5406Å) and verified by cross-section TEM measurements. While X-ray diffraction yields information on the structural properties averaging over a macroscopic region, HRTEM gives information on the local crystal structure with atomic resolution. All the crystallographic planes and directions of LBM films used in this work are indexed according to orthorhombic notation and crystallite sizes are determined by using Scherrer equation ($\tau = k\lambda/\beta\cos\theta$), assuming k = 0.94 for cubic crystallites. The MPMS-3 superconducting quantum interface device (SQUID) magnetometer was used to study the magnetic properties, in temperature range of 10–350 K and magnetic field up to 2 T. The cross-sectional TEM specimens investigated in this experiment were prepared by mechanical grinding to a thickness of about 10 μm, and then Ar ion milling to reach electron transparency using a Precision Ion Polishing system. HRTEM experiments were done in a JEOL 2200 FS 200 kV FEG, equipped with energy filter and EDS detector and a FEI TITAN80–300 kV with Cs corrector and EDS and HAADF detectors. HAADF and bright field STEM images were taken in the dedicated STEM Hitachi HD2700 equipped with EDS Bruker and nano-diffraction, operated at 200 kV.

3. Results and discussion

Fig. 1 shows X-ray-diffraction patterns (θ–2θ scan) obtained for two single layer LBM thin films and two LBMBT heterostructures grown on [0001]- Al_2O_3 and [100]-Si substrates. The subscripts "a" and "s" are the indication of the Al_2O_3 and Si substrate, respectively. The LBM_a thin film adopts the rhombohedral space group with R-3c symmetry following c-axis of substrate, due to the strain from the LBM/substrate interface (PDF file number: 04-013-5744). The (00l) peaks in XRD pattern indicates that the LBM_a film follows c-oriented growth with c_{film}= 13.5096Å, while extra (012) peak family appears in XRD pattern giving a_{film}= 5.5221Å, Fig. 1(a). Therefore, LBM_a experiences an in-plane tensile strain in-plane= 16.08%). From the X-ray in-plane and out-of-plane measurements, distortion ratios are calculated as ε_{xx}=−0.61% and ε_{zz}= 0.43%. These distortions can be used to evaluate the Poisson coefficient ν of the film, $\varepsilon_{zz} = [(\nu - 1)/2\nu]\,\varepsilon_{xx}$ [23], which gives ν = 0.41 for the film. This can be compared to previous studies onLa1−xBaxMnO3film [24]. $LBMBT_a$ heterostructure is also following c-plane growth, while extra diffraction peaks appear at 2θ = 32.35° ,2θ = 38.65° and 2θ = 83.08°, corresponding to (104) peak of rhombohedral top LBM layer, hexagonal BaTiO3(003) and (006) [25], respectively, Fig. 1(b). The $BaTiO_3$ layer growth shows hexagonal space group with c = 7.000Å, (PDF file number: 01-073-7322).

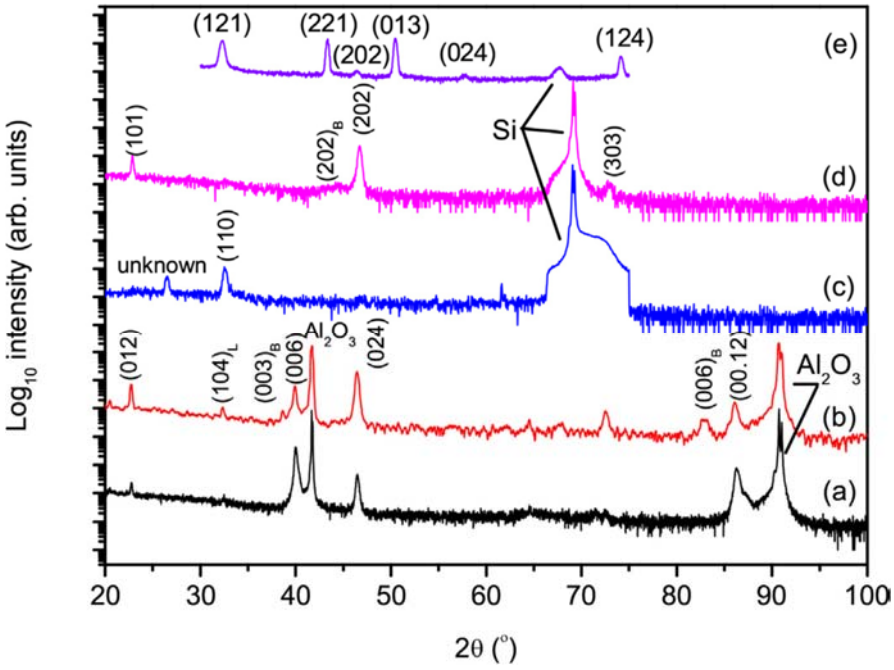

Figure 1.Fig. 1. X-ray-diffraction pattern (ϑ–2ϑ scan) of two single layers of LBM films on Al_2O_3 and Si substrate as well as of two LBMBT heterostructures: (a) 50-nm-thick LBM film on Al_2O_3 substrate; (b) LBM (40 nm)/$BaTiO_3$(30 nm)/LBM (40 nm) on Al_2O_3 substrate; (c) 145-nm-thick LBM film on Si substrate; (d) LBM (40 nm)/$BaTiO_3$(30 nm)/LBM (40 nm) on Si substrate, where L and B indices refer to the top LBM and$BaTiO_3$ layers, and (e) asymmetrical XRD pattern of $LBMBT_s$ heterostructure.

The LBM_s thin film presents different crystal structure than LBM_a thin film, as shown in Fig. 1(c). The (110) diffraction peak is assigned as main diffraction peak in single layer, where the peak at $2\theta = 26.54^\circ$ does not match any peak in database. Mean-while, $LBMBT_s$ heterostructure presents b-oriented growth on (100) Si with (l0l) family group in diffraction pattern, which are associated with *Pnma* orthorhombic space group with a = 5.5079Å, b = 7.816Å and c = 5.5516Å, Fig. 1(d) (PDF file number: 04-006-8863). Also, asymmetrical X-ray measurements present (121) and (221) diffraction peaks in LBM layer, Fig. 1(e). From diffraction peaks at $2\theta = 22.75^\circ$, 32.35° and 43.37° corresponds to cell parameter of a = 5.4954Å, b = 7.8206Å and c = 5.5656Å. Therefore, the first LBM layer feels in-plane tensile strain ($\delta_{in\text{-}plane}$= 1.2%) in a-direction and ($\delta_{in\text{-}plane}$= 2.5%) in c-direction. As the LBM film being deposited on Si substrate, the in-plane lattice tends to adopt the structure of Si and the out-of-plane parameter reacts correspondingly to maintain unit cell volume. It is possible to calculate in-plane and out-of-plane distortion ratios as: ε_{xx}=−0.22%, ε_{yy} = 0.26% and ε_{zz} = 0.06%. $BaTiO_3$ layer is deposited on the (l0l)- oriented LBM layer, adapting its structure to hexagonal space group with a = b = 5.700Å and c = 7.000Å.

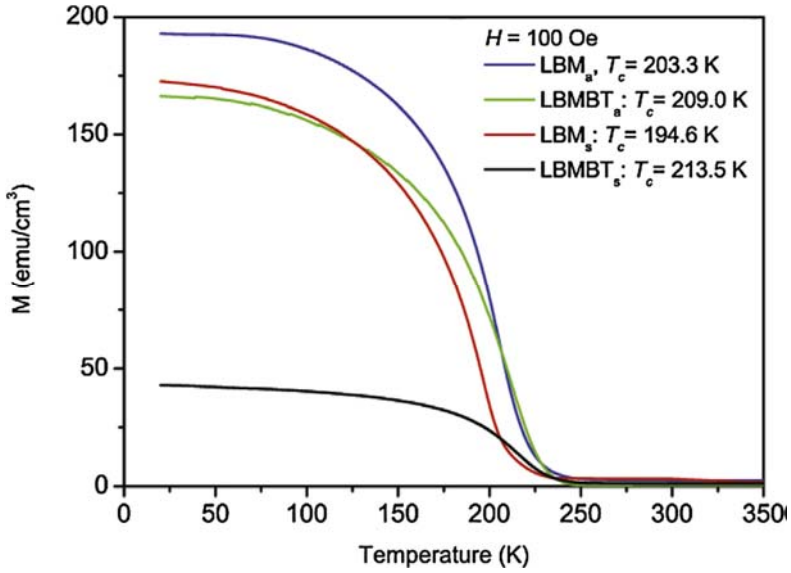

Figure 2. Temperature dependence of the magnetization of LBM_a, LBM_s thin films, $LBMBT_a$ and $LBMBT_s$ heterostructures. LBM_a and $LBMBT_s$ present the highest and lowest magnetization at T = 20 K, respectively.

The temperature dependence of the magnetization in the single layers and heterostructure was measured under applied field H = 100 Oe for field-cooling and results are presented in Fig. 2. Curie temperature associated with transition from ferromagnetic to paramagnetic phase is defined as the temperature where |dM/dT| is minimum in the M–T curves shown in Fig. 2. Although the increase in T_C from single layer to heterostructure is obvious in both substrates (~6 K for Al_2O_3 substrate and ~20 K for Si substrate), the difference in the values is related to the structural changes and lattice mismatch in films. Comparing the T_C value for all the stressed samples LBM_s has the lowest one (T_C = 194.6 K), which can be related to higher compressive strain imposed by the substrate [5]. Also, measured magnetization at T = 20 K of the films and heterostructures reveal the highest magnetization corresponds to LBM_a film.

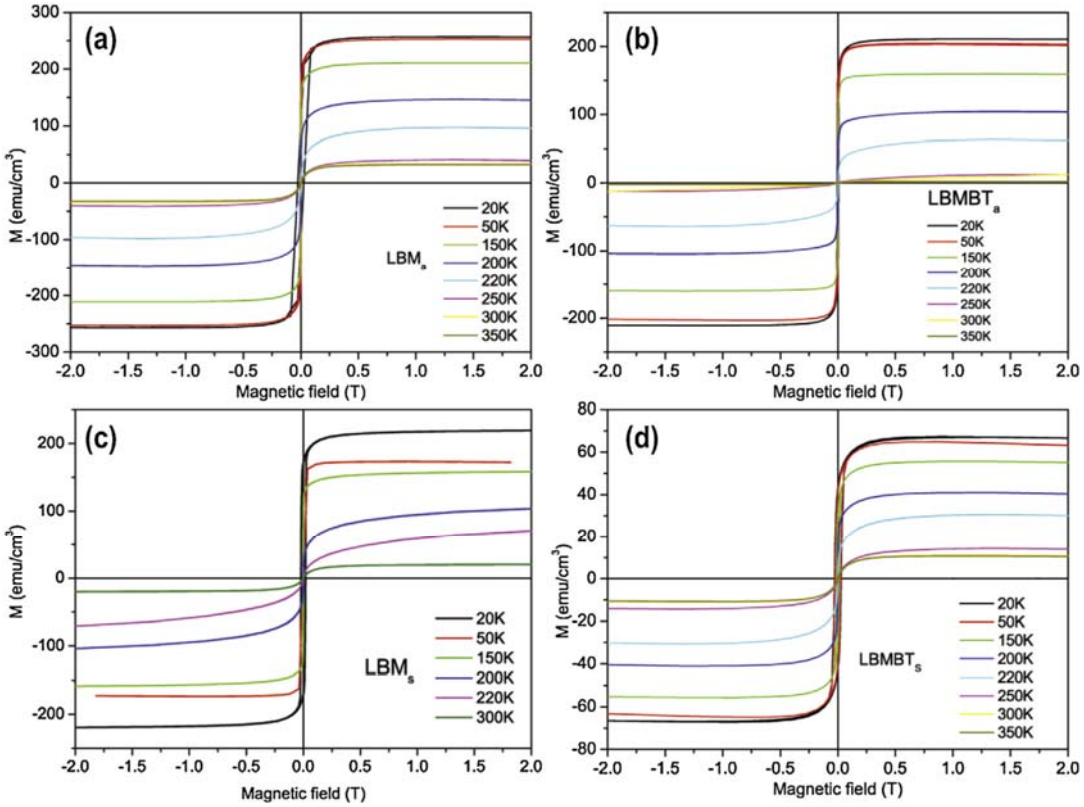

Figure 3. Magnetic hysteresis cycles of (a) LBM_a thin film, (b) $LBMBT_a$ heterostructure, (c) LBM_s thin film and (d) $LBMBT_s$ heterostructure.

Fig. 3 shows the hysteresis loops (M–H) of the samples after subtracting diamagnetic contribution of the substrate, measured at different temperatures with the applied magnetic field parallel to the substrate plane. The highest magnetization value under applied field of H = 2T corresponds to LBM_a single layer with M ~ 256.7 emu/cm^3 at T = 20 K, Fig. 4(a), which does not reach the spontaneous magnetization of polycrystalline bulk $La_{0.9}Ba_{0.1}MnO_3$ ~ 100 emu/g (~600 emu/cm^3) [15]. The decrease in M may be related to several factors, including possible rearrangement in the Mn O bond length/angle due to the internal strain [5,26], oxygen deficiency in film [27], crystal structure of the film, etc. Also, hysteresis cycles show that $LBMBT_s$ has highest coercivity, H_c~310 Oe at T = 20 K, as shown in Fig. 4(b) indicating all the samples are soft magnets.

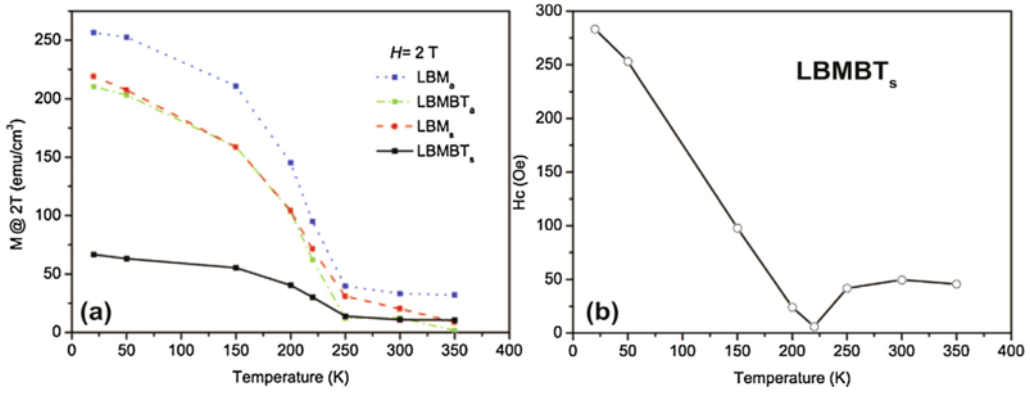

Figure 4. (a) Temperature dependence of the magnetization of LBM_a, LBMs thin films, $LBMBT_a$ and $LBMBT_s$ heterostructures, under applied field of 2T. LBM_a and $LBMBT_s$ present the highest and lowest magnetization at T = 20 K, respectively. (b) Time dependence of coercivity of $LBMBT_s$ shows the highest H_c, proves that thin films and heterostructures are soft magnets.

Dependency of T_C to strain in lattice of $La_{1-x}Ba_xMnO_3$ ($0.05 \leq x \leq 0.33$) thin films was already shown [5,28]. For the low doped films ($x \leq 0.2$), tensile strain was calculated with enhancement of ferromagnetic transition temperature (T_C). All low doped films showed T_C greater than the one for corresponding bulk composition. As film thickness was increasing, the out-of-plane parameter of the lattice increased, reaching the value of the bulk, whereas the in-plane tensile strain and T_C both decreased. Beside of double exchange mechanism via electron hopping through Mn^{3+}-O^{2-}-Mn^{4+} paths, dependency of T_C to in-plane tensile strain was assigned to elongation of Mn O bond distance. In-plane elongation of Mn O bonds in turn will stabilize d_{x2-y2} character in the occupied e_g state, and consequently enhances electron hopping and double exchange interaction in the strained films. Our calculated T_C of heterostructure on Al_2O_3 (209 K) with in-plane strain of −2.9% is greater than the T_C of single layer (203 K) with slightly lower tensile strain, −2.72%. However, high T_C value (213 K) of grown heterostructure on silicon substrate with in-plane compressive strain of 1.2% does not match with above hypothesis. This inconsistency on describing the trend of T_C driven by strain in films was assigned to the primarily effect of change in bond angle in Mn^{3+}-O^{2-}-Mn^{4+} network under tensile or compressive strains [26]. Beside of purely geometrical factors, electron–phonon coupling was considered to give more accurate trend of T_C in strained films of manganite [26]. Recent observation of behavior of T_C in films of $La_{0.9}Sr_{0.1}MnO_3$ deposited on three different substrates which imposes films to either tensile or compressive strains did reveal more complex connection of T_C and the state of the strain in the films [29]. Depends on the substrate, MgO or $SrTiO_3$, although both impose films to tensile strain, T_C can be either higher or lower than the T_C of the compressive strained film deposited on $LaAlO_3$ substrate [29]. This study reveals the necessity of considering change in both Mn O bond distance and Mn O Mn bond angle for a qualitative explanation of trend in T_C under strain effect, more elaborated than previous explanations. Calculated high T_C value of the deposited heterostructure on silicon in our work with compressive strain in compare to those deposited on Al_2O_3 substrate with tensile strain may originate from complex distortion of the lattice due to different factors in the films. Since growth orientation, nanostructure of the film and composition shift can affect the distortion of MnO_6 octahedral, we have performed TEM analysis of the grown films to catch any dis-ordering at the interface and to explore the nanostructure of the films.

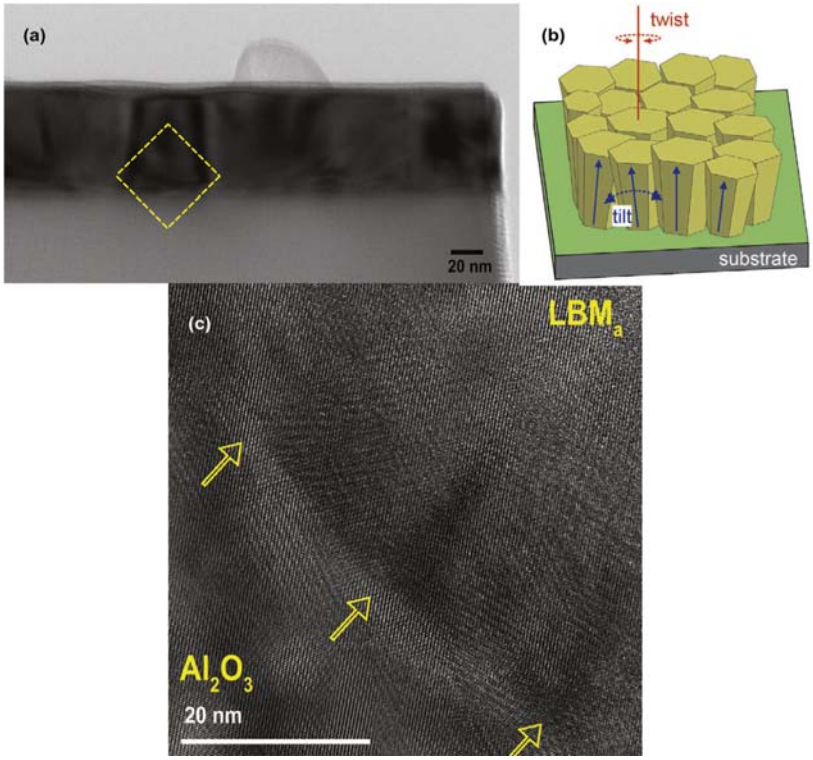

Figure 5. TEM micrograph of the LBM$_a$ film on Al2O3substrate, (a) bright field image shows the mosaic structure in the grown film and (b) HRTEM of LBM$_a$ thin film presents the epitaxial growth on the substrate. (c) Arrows mark the twisting in mosaic structure of the film.

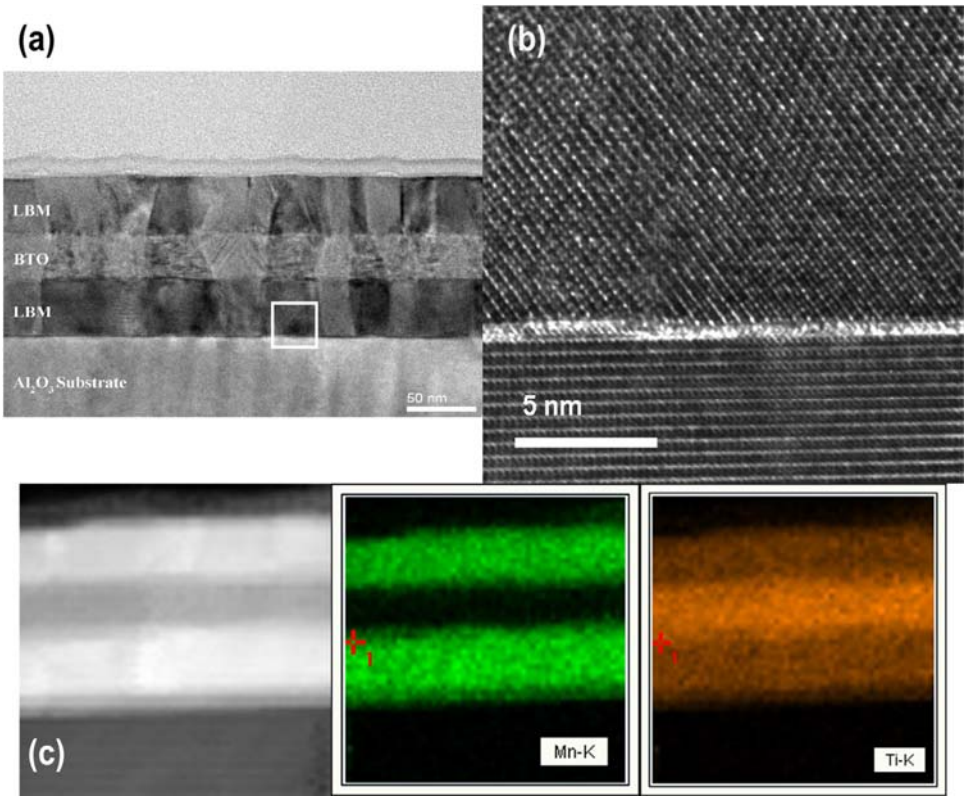

Figure 6. (a) TEM micrograph of LBMBT$_a$ heterostructure, the thickness of the layers is 40/30/40 nm, respectively, (b) the interface between bottom LBM layer and substrate, the epitaxial growth of the film is obvious, and (c) the STEM-HAADF micrograph and EELS- mapping of the LBMBT$_a$ heterostructure.

Therefore, to shed light on the interplay of strain, chemistry shift and defects in the films on magnetic properties, also our difficulty in phase identification of LBM_s, high resolution TEM was done on all the samples. Fig. 5(a) shows flat surface of ~50 nm-thick LBM_a crystalline film on Al_2O_3 substrate. The mosaic structure in film structure reveals (220) oriented epitaxial growth inside each mosaic, twisted with respect to the adjacent mosaic, Fig. 5(c). Drawing attention to the film/substrate interface an expected sharp interface is missing, which can be attributed to inhomogeneity on provided substrate surface and deposition parameters, especially substrate temperature and deposition time providing a possible diffusion of film into the substrate. Also, the starting point of mosaics are marked with arrows in Fig. 5(c), showing mosaics with aver-age lateral size of 32.1 nm, well corroborated with value of 36.5 nm calculated from (006) reflection peak in Fig. 1(c) using Scherrer equation [30]. Beside of strain effect on T_C, the size of nanocrystalline mosaic observed in TEM was reported to change T_C of $La_{0.7}Sr_{0.3}MnO_3$ on $SrTiO_3$/Si [31–33]. The reduced size of nanocrystallites in our LBM films can minimize the strain effect, which duly increase T_C.

The mosaic structure is also visible in $LBMBT_a$ heterostructure through all three layers, Fig. 6(a). However, small bending of boundaries is seen in $BaTiO_3$ and top LBM layer, because of difference in lattice parameters of films inducing non-uniform strain during growth. The substrate/film interface within one of mosaics is shown in Fig. 6(b), indicating epitaxial growth of (001) planes of film along (001) axis of substrate, also indicated by XRD, Fig. 1(c). While first LBM layer shows highly oriented epitaxial film, the $BaTiO_3$ and top LBM layer present lower crystallinity. Also, average lateral size of mosaics in different layers are measured as 31.73 nm in bottom LBM, 34.6 nm in $BaTiO_3$ and 31.84 nm in top LBM layer matching the grain size of (006) LBM, (003) BaTiO3and (121) LBM, respectively. STEM-HAADF micrograph and EELS-mapping analysis of $LBMBT_a$ heterostructure clarify the diffusion of Ti atoms from $BaTiO_3$ layer into LBM layers, Fig. 6(c). Considering the mosaic structure, the strain near mosaic boundaries is an additional factor in changing magnetic properties of films and heterostructures [34,31].

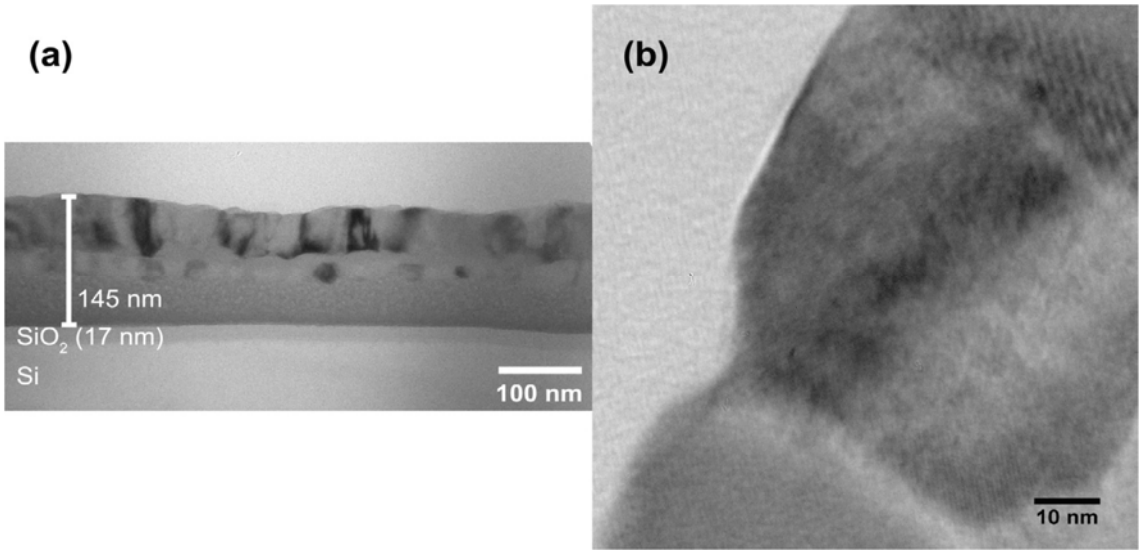

Figure 7. (a) TEM micrograph of LBM_s thin film and (b) grain structure and the crystallized region of film surface.

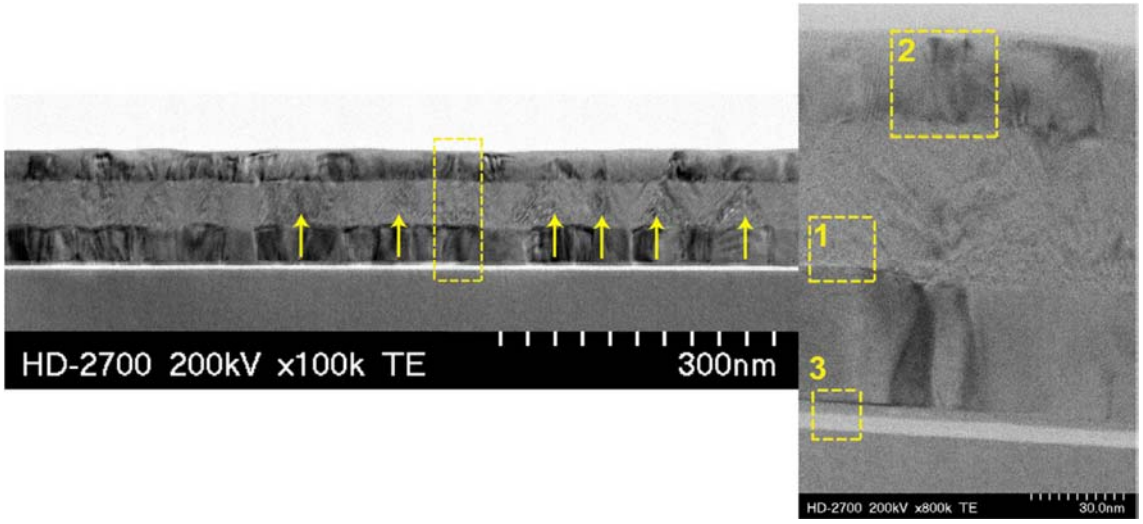

Figure 8. STEM micrograph of $LBMBT_s$ heterostructure on Si/SiO_2 substrate shows mosaic structure along the heterostructure. Arrows indicate the strain in $BaTiO_3$ caused by mosaic structure in first LBM layer.

On the other hand, TEM results of LBM_s single layer in Fig. 7 shows peculiar crystalline behavior as growth proceeds. The film microstructure altered from completely amorphous structure over a 17 nm-layer of SiO_2 to mosaic crystalline structure. As expected from previous studies [35,36], lower crystallinity in LBM_s film in comparison with LBM_a single layer affects the magnetization of the film and diminishes it. Likewise, STEM analysis of $LBMBT_s$ in Fig. 8 presents crystallinity on first LBM layer (Fig. 9(1)) with some mosaic structure, with average mosaic size of 42.7 nm. Unlike $LBMBT_a$ heterostructure, the mosaic structure does not continue through $BaTiO_3$ layer but reappears in top LBM layer, where the average mosaic size decreases to 26.6 nm compared to first LBM layer. Instead, some traces of stress can be seen in $BaTiO_3$ layer, starting from corner of mosaics in first LBM layer and ends to the corners in top LBM layer, marked by arrows in Fig. 8. This was expected from the XRD results, where the strain in $LBM/BaTiO_3$ interface is different in $LBMBT_a$ and $LBMBT_s$, due to different space group of bottom LBM layer. Also, lower crystalline mosaic structure of top LBM layer is visible. Another feature appears in the inter-face of substrate with first LBM layer, where in addition to SiO_2 layer the existence of an extra layer with different layer density is observed, Fig. 9(3). This layer is continuous along the interface and does not present any mosaic structure. The existence of such a layer was observed before on manganite layers on oxide substrate, which found to be weak ferromagnetic or even antiferromagnetic [37].

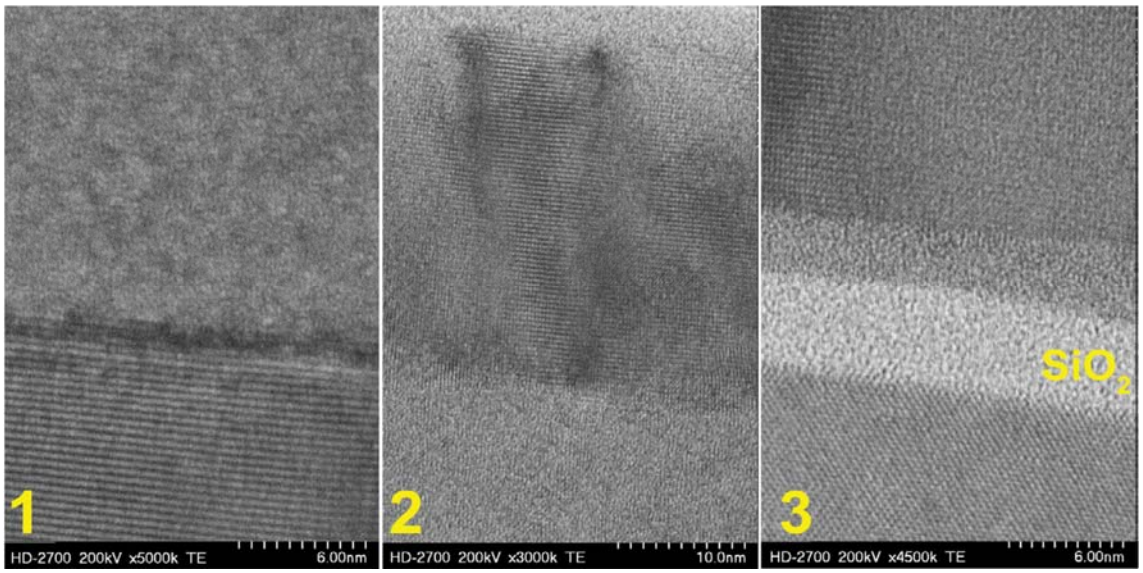

Figure 9. STEM micrograph of interfaces in LBMBT$_s$ heterostructure marked in Fig. 8 shows the crystalline growth of bottom LBM layer (1) and amorphous BTO layer (1 and 2) and crystalline top LBM layer (2). Also, existence of a layer is approved on top of SiO_2 layer (3).

In summary, dependence of magnetization and T_C of LBM films on their microstructure has been studied. The reduction in T_C from LBM$_a$ to LBM$_s$ is explained by increasing the compressive strain between film and substrate. Also, the T_C can be affected by observed mosaic structure in the films and heterostructures by width of~30 nm. The existence of the boundaries in mosaic structure can reduce the strain effect through strain relaxation at the interface and results in reduction of magnetization and T_C in manganite films [31,32]. The magnetization value in heterostructures decreased in comparison with single layer films on the same substrate, while T_C increased in both substrates. Although the understanding the role of crystallinity on magnetization of single layers is easy, it is not simple to describe the magnetic behavior in heterostructures as the effect of interfaces with the intermediate $BaTiO_3$ layer should be considered. The first LBM layer experiences the strain induced by the substrate, where the top LBM layer is growing on strained $BaTiO_3$ layer. As the structure of $BaTiO_3$ layer depends strictly on the structure of first LBM layer, it affects the structure of top LBM layer. The lowest magnetization in LBMBT$_s$ heterostructure is attributed to the crystallinity of LBM layers, where more defects are created in manganite layers due to the diffusion of Ti ions into ferromagnetic layers. Therefore, it is safe to say that beside of strain, chemistry shift and nanocrystalline mosaic structure can play important roles on magnetic properties of the films and heterostructures.

4. Conclusions

We have investigated the structural and magnetic properties of LBM thin films and LBMBT heterostructures on Al_2O_3 and Si substrates. The rhombohedral grown thin film and heterostructure on Al_2O_3 substrate show out of plane compressive strain in substrate/film interface, while $BaTiO_3$ presents hexagonal space group. LBMBT heterostructure on Si substrate adopts orthorhombic phase with tensile strain in out of plane lattice parameter. TEM/STEM images of the films have revealed formation of

mosaic structure with nanocrystallites orientated along growth direction. The lateral size of the nanocrystallites ranges from 25 nm to 45 nm indifferent layers, where the finest value belongs to the top LBM layer in $LBMBT_s$ heterostructure. EELS-mapping was used to determine chemistry shift in $LBMBT_a$ heterostructure, where diffusion of Ti ions from intermediary $BaTiO_3$ layer into magnetic LBM layers was seen. Compared to the bulk structures, T_C of all grown films show obvious enhancement. The direct effect of tensile/compressive strain in films on magnetic properties was discussed. It was concluded that in addition to the strain/stress in the films, transition metal diffusion, oxygen deficiency and fine lateral size of the nanocrystallites in the structure of the films should be taken into account for a comprehensive understanding of the magnetic properties of the deposited $La_{0.9}Ba_{0.1}MnO_3$ films.

Acknowledgments

This work was developed in the scope of the project CICECO-Aveiro Institute of Materials (Ref. FCT UID/CTM/50011/2013), financed by national funds through the FCT/MEC and when applicable co-financed by FEDER under the PT2020 Partnership Agreement. We would like to thank the financial support from the FCT project PTDC/FIS/105416/2008 "MUL-TIFOX" and PTDC/CTM/099415/2008 grants and FCT project SFRH/BD/51140/2010 in order to access all microscopes in pole of electron microscopy in Aveiro University.

References

[1] M. Fiebig, Revival of the magnetoelectric effect, J. Phys. D: Appl. Phys. 38 (8)(2005) R123–R152, http://dx.doi.org/10.1088/0022-3727/38/8/r01.

[2] W. Eerenstein, N.D. Mathur, J.F. Scott, Multiferroic and magnetoelectric materials, Nature 442 (7104) (2006) 759–765, http://dx.doi.org/10.1038/nature05023.

[3] R.E. Cohen, Origin of ferroelectricity in perovskite oxides, Nature 358 (6382)(1992) 136–138, http://dx.doi.org/10.1038/358136a0.

[4] S.P. Alpay, V. Nagarajan, J. Rossetti, Recent developments in ferroelectric nanostructures and multilayers, J. Mater. Sci. 44 (19) (2009) 5021–5024,http://dx.doi.org/10.1007/s10853-009-3788-x.

[5] J. Zhang, H. Tanaka, T. Kanki, J.H. Choi, T. Kawai, Strain effect and the phase diagram of $La_{1-x}Ba_xMnO_3$ thin films, Phys. Rev. B 64 (18) (2001) 6275–6279,http://dx.doi.org/10.1103/PhysRevB.64.184404.

[6] R. Vonhelmolt, J. Wecker, B. Holzapfel, L. Schultz, K. Samwer, Giant negative magnetoresistance in perovskite like $La_{2/3}Ba_{1/3}MnO_X$ ferromagnetic-films, Phys. Rev. Lett. 71 (14) (1993) 2331–2333, http://dx.doi.org/10.1103/PhysRevLett.71.2331.

[7] H.L. Ju, Y.S. Nam, J.E. Lee, H.S. Shin, Anomalous magnetic properties and magnetic phase diagram of $La_{1-x}Ba_xMnO_3$, J. Magn. Magn. Mater. 219 (1)(2000) 1–8, http://dx.doi.org/10.1016/s0304-8853(00)00429-7.

[8] S.-W. Cheong, M. Mostovoy, Multiferroics: a magnetic twist for ferroelectricity, Nat. Mater. 6 (1) (2007) 13–20, http://dx.doi.org/10.1038/nmat1804.

[9] N.A. Spaldin, S.-W. Cheong, R. Ramesh, Multiferroics: past, present, and future, Phys. Today 63 (10) (2010) 38–43.

[10] L.W. Martin, S.P. Crane, Y.H. Chu, M.B. Holcomb, M. Gajek, M. Huijben, C.H.Yang, N. Balke, R. Ramesh, Multiferroics and magnetoelectrics: thin films and nanostructures, J. Phys.: Condens. Matter 20 (43) (2008) 434220, http://dx.doi.org/10.1088/0953-8984/20/43/434220.

[11] H.Y. Hwang, S.W. Cheong, P.G. Radaelli, M. Marezio, B. Batlogg, Lattice effects on the magnetoresistance in doped $LaMnO_3$, Phys. Rev. Lett. 75 (5) (1995)914–917, http://dx.doi.org/10.1103/PhysRevLett.75.914.

[12] H. Lu, C.W. Bark, D.E. de los Ojos, J. Alcala, C.B. Eom, G. Catalan, A. Gruverman, Mechanical writing of ferroelectric polarization, Science 336 (6077) (2012)59–61, http://dx.doi.org/10.1126/science.1218693.

[13] A. Biswas, M. Rajeswari, R.C. Srivastava, Y.H. Li, T. Venkatesan, R.L. Greene, A.J. Millis, Two-phase behavior in strained thin films of hole-doped manganites, Phys. Rev. B 61 (14) (2000) 9665–9668, http://dx.doi.org/10.1103/PhysRevB.61.9665.

[14] A.J. Millis, P.B. Littlewood, B.I. Shraiman, Double exchange alone does not explain the resistivity of $La_{1-x}Sr_xMnO_3$, Phys. Rev. Lett. 74 (25) (1995)5144–5147, http://dx.doi.org/10.1103/PhysRevLett.74.5144.

[15] R.C. Budhani, C. Roy, L.H. Lewis, Q.A. Li, A.R. Moodenbaugh, Magnetic ordering and granularity effects in $La_{1-x}Ba_xMnO_3$, J. Appl. Phys. 87 (5) (2000)2490–2496, http://dx.doi.org/10.1063/1.372208.

[16] Q.X. Zhu, M. Zheng, M.M. Yang, X.M. Li, Y. Wang, X. Shi, H.L.W. Chan, H.S. Luo, X.G. Li, R.K. Zheng, Effects of ferroelectric-poling-induced strain on magnetic and transport properties of $La_{0.67}Ba_{0.33}MnO_3$ thin films grown on (111)-oriented ferroelectric substrates, Appl. Phys. Lett. 103 (13) (2013),http://dx.doi.org/10.1063/1.4822269.

[17] Y.F. Lu, J. Klein, C. Hofener, B. Wiedenhorst, J.B. Philipp, F. Herbstritt, A. Marx, L. Alff, R. Gross, Magnetoresistance of coherently strained $La_{2/3}Ba_{1/3}MnO_3/SrTiO_3$ superlattices, Phys. Rev. B 62 (23) (2000)15806–15814, http://dx.doi.org/10.1103/PhysRevB.62.15806.

[18] T. Kanki, H. Tanaka, T. Kawai, Enhancement of magnetoresistance at room temperature in $La_{0.8}Ba_{0.2}MnO_3$ epitaxial thin film, Solid State Commun. 114(5) (2000) 267–270, http://dx.doi.org/10.1016/s0038-1098(00)00038-7.

[19] J. Zhang, A.A. Heitmann, S.P. Alpay, G.A. Rossetti, Electrothermal properties of perovskite ferroelectric films, J. Mater. Sci. 44 (19) (2009) 5263–5273, http://dx.doi.org/10.1007/s10853-009-3559-8.

[20] P.-E. Janolin, Strain on ferroelectric thin films, J. Mater. Sci. 44 (19) (2009)5025–5048, http://dx.doi.org/10.1007/s10853-009-3553-1.

[21] M. Mayer, SIMNRA, a simulation program for the analysis of NRA, RBS and ERDA, in: 15th International Conference on the Application of Accelerators in Research and Industry, vol. 475 of AIP Conference Proceedings, 1999, pp.541–544.

[22] R.C. Bird, J.S. Williams, Ion Beams for Materials Analysis, Elsevier, 1990.

[23] L. Ranno, A. Llobet, R. Tiron, E. Favre-Nicolin, Strain-induced magnetic anisotropy in epitaxial manganite films, Appl. Surf. Sci. 188 (1-2) (2002)170–175, http://dx.doi.org/10.1016/s0169-4332(01)00730-9.

[24] Y.-C. Liang, Y.-C. Liang, Quantifying strain effects on physical properties of $La_{0.68}Ba_{0.32}MnO_3$ epilayers and heterostructures, J. Electrochem. Soc. 154 (12)(2007) P147–P151, http://dx.doi.org/10.1149/1.2789293.

[25] V.A. Cherepanov, E.A. Filonova, V.I. Voronin, I.F. Berger, Phase equilibria in the $LaCoO_3$–$LaMnO_3$–$BaCoO_z$–$BaMnO_3$ system, J. Solid State Chem. 153 (2) (2000)205–211, http://dx.doi.org/10.1006/jssc.2000.8743.

[26] Q.S. Yuan, Comment on "Strain effect and the phase diagram of $La_{1-x}Ba_xMnO_3$ thin films, Phys. Rev. B 70 (6) (2004), http://dx.doi.org/10.1103/PhysRevB.70.066401.

[27] J. Fang, Y. Cui, Magnetic and transport properties of samples of the approximate composition $La_{0.9}Ba_{0.1}MnO_3$ with different cation deficiencies, J. Alloys Compd. 432 (1-2) (2007) 15–17, http://dx.doi.org/10.1016/j.jallcom.2006.05.125.

[28] J. Zhang, H. Tanaka, T. Kawai, Strain-induced insulator-metal transition and room-temperature colossal magnetoresistance in low-doped $La_{1-x}Ba_xMnO_3$ thin films, J. Appl. Phys. 90 (12) (2001) 6275–6279, http://dx.doi.org/10.1063/1.1416866.

[29] L. Yin, C. Wang, Q. Shen, L. Zhang, Strain-induced Curie temperature variation in $La_{0.9}Sr_{0.1}MnO_3$ thin films, RSC Adv. 6 (98) (2016) 96093–96102, http://dx.doi.org/10.1039/c6ra22392c.

[30] B.D. Cullity, Introduction to Magnetic Materials, 2nd edition, Wiley, 2009.

[31] A.K. Pradhan, J.B. Dadson, D. Hunter, K. Zhang, S. Mohanty, E.M. Jackson, B.Lasley-Hunter, K. Lord, T.M. Williams, R.R. Rakhimov, J. Zhang, D.J. Sellmyer,K. Inaba, T. Hasegawa, S. Mathews, B. Joseph, B.R. Sekhar, U.N. Roy, Y. Cui, A.Burger, Ferromagnetic properties of epitaxial manganite films on $SrTiO_3$/Si heterostructures, J. Appl. Phys. 100 (3) (2006), http://dx.doi.org/10.1063/1.2222402.

[32] A.K. Pradhan, S. Mohanty, K. Zhang, J.B. Dadson, E.M. Jackson, D. Hunter, R.R.Rakhimov, G.B. Loutts, J. Zhang, D.J. Sellmyer, Integration of epitaxial colossal magnetoresistive films onto Si(100) using $SrTiO_3$ as a template layer, Appl. Phys. Lett. 86 (1) (2005), http://dx.doi.org/10.1063/1.1842852.

[33] S.K. Mandal, T.K. Nath, V.V. Rao, Effect of nanometric grain size on electronic-transport, magneto-transport and magnetic properties of $La_{0.7}Ba_{0.3}MnO_3$ nanoparticles, J. Phys.: Condens. Matter 20 (38) (2008), http://dx.doi.org/10.1088/0953-8984/20/38/385203.

[34] S. Farokhipoor, C. Magen, S. Venkatesan, J. Iniguez, C.J.M. Daumont, D. Rubi, E.Snoeck, M. Mostovoy, C. de Graaf, A. Mueller, M. Doeblinger, C. Scheu, B. Noheda, Artificial chemical and magnetic structure at the domain walls of an epitaxial oxide, Nature 515 (7527) (2014) 379, http://dx.doi.org/10.1038/nature13918.

[35] J. Zippel, M. Lorenz, A. Setzer, M. Rothermel, D. Spemann, P. Esquinazi, M. Grundmann, G. Wagner, R. Denecke, A.A. Timopheev, Defect-induced magnetism in homoepitaxial manganese-stabilized zirconia thin films, J. Phys. D: Appl. Phys. 46 (27) (2013), http://dx.doi.org/10.1088/0022-3727/46/27/275002.

[36] M. Li, G.C. Wang, H.G. Min, Effect of surface roughness on magnetic properties of Co films on plasma-etched Si (100) substrates, J. Appl. Phys. 83 (10) (1998)5313–5320, http://dx.doi.org/10.1063/1.367357.

[37] W. Luo, S.J. Pennycook, S.T. Pantelides, Magnetic "dead" layer at a complex oxide interface, Phys. Rev. Lett. 101 (24) (2008), http://dx.doi.org/10.1103/PhysRevLett.101.247204

.